Dispersion of surface acoustic waves in thin films at extreme wavelength-to-thickness ratios

Marc Duquennoy, Tahar Kadi, Mohammadi Ouaftouh, Nikolay Smagin, Frédéric Jenot

JASA EXPRESS LETTERS ARTICLE asa.scitation.org/journal/jel

Dispersion of surface acoustic waves in thin films at extreme wavelength-to-thickness ratios

Marc Duquennoy,[a] **Tahar Kadi, Mohammadi Ouaftouh, Nikolay Smagin, and Frederic Jenot**
IEMN (UMR CNRS 8520), Université Polytechnique Hauts-de-France, CNRS, Université Lille, F-59313 Valenciennes, France
marc.duquennoy@uphf.fr, kadi.tahar@etu.uphf.fr, mohammadi.ouaftouh@uphf.fr, nikolay.smagin@uphf.fr, frederic.jenot@uphf.fr

Abstract: Surface acoustic waves (SAWs) are sensitive to the presence of a layer on the surface of a material, even if this layer is extremely thin compared to their wavelengths. Given the very slow propagation velocities of SAWs compared to electromagnetic waves, their wavelengths are on the order of 40 μm for acoustic frequencies on the order of 100 MHz. However, it has been shown that these waves are dispersive for coatings whose thicknesses are more than 1000 times smaller than their wavelength. This sensitivity is verified by studying the dispersion of SAWs for a frequency range between 90 and 260 MHz.

[Editor: Joel Mobley] https://doi.org/10.1121/10.0014859

Received: 10 July 2022 **Accepted:** 30 September 2022 **Published Online:** 25 October 2022

In this study, very high-frequency surface acoustic waves (SAWs) were generated over a wide frequency band between 90 and 260 MHz using remote interdigital transducers (IDTs). The controlled excitation of SAWs over a wide frequency band is essential to demonstrate the dispersion of SAWs in thin films with extreme wavelength-to-thickness ratios. Several techniques have been used to generate Rayleigh type surface waves, including laser-ultrasound (Goossens *et al.*, 2007; Lomonosov *et al.*, 2001; Ruiz and Nagy, 2003), wedges (Tittmann *et al.*, 1987), immerged transducers (Lakestani *et al.*, 1995), line-focus acoustic transducers (Warren *et al.*, 1996), or IDTs (Deboucq *et al.*, 2011; Duquennoy *et al.*, 2012; Fall *et al.*, 2016). The latter allow broadband SAW generation on a piezoelectric substrate in an easily controllable way using a chirped electrode finger configuration (Tancrell and Holland, 1971). Since IDTs are offset transducers for non-destructive testing (NDT) applications, it is necessary to provide sustainable acoustical contact with the structure under test. This issue is sometimes circumvented by integrating IDT electrodes and the piezoelectric substrate directly into the structure (Toda *et al.*, 1994; Wu *et al.*, 2005), leading, on the other hand, to unavoidable limitations in the configurations of the samples to be characterized. Excitation with interdigital transducers not only allows SAWs to be generated on any structure, even if it is a fragile and/or transparent one, but also allows SAWs to be generated with large displacement amplitudes over the entire frequency band (Fall *et al.*, 2016, 2017, 2018a). The optimization of IDTs specially designed for SAW excitation was favored (Fall *et al.*, 2018a). Indeed, SAW generation using remote IDTs is a major asset in this study as it is non-destructive and can be used for any type of coating (metallic, polymer, etc.). No prior preparation of the structures on which the SAWs are to be propagated is necessary, unlike with other methods (Hess, 2009; Schneider *et al.*, 1999). Only coupling with a very thin liquid film is required (Fall *et al.*, 2018b). The layers are extremely thin, and their influence is small, so to observe a variation in the velocity of several m/s it is necessary to observe the dispersion of SAWs over a wide frequency band, which is why this ability to efficiently generate SAWs over a wide frequency band is essential.

In the experimental setup (Fig. 1) the 3-in. silicon wafers on which the chromium layers were deposited were fixed to a motorized XY table (300 nm of displacement resolution). The SAW-IDT is placed flat and maintained on the sample with a couplant. The transducer surface, on which the fingers are deposited, is in contact with the sample. The surface wave generated by the IDT propagates perpendicularly to the fingers along the surface of the piezoelectric $LiNbO_3$ substrate on which the comb has been deposited. In the area where the piezoelectric substrate and the sample are in contact, the wave is transmitted and then propagates in the sample. This contact allowed us to carry out several sets of measurements at different points of detection on the sample while maintaining the same coupling between the SAW-IDT micro-electrical-mechanical system (MEMS) and the sample. The signal received by the vibrometer photodiode was digitized using a LeCroy (Chestnut Ridge, NY) 725Zi-A oscilloscope and transferred to a personal computer (PC) for digital IQ demodulation. The chirp-like excitations of the IDTs were generated using a Tektronix (Beaverton, OR) 7051 arbitrary waveform generator. The signal voltage was increased to 20 V using a 50 W/1000 A power amplifier from Amplifier

[a]Author to whom correspondence should be addressed.

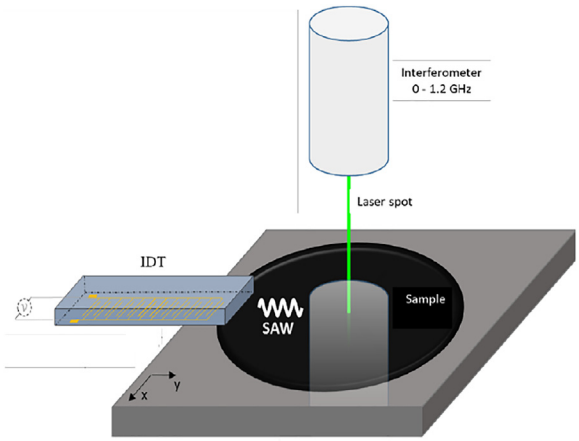

Fig. 1. Diagram of the experimental setup including SAW excitation and detection.

Research (Fall *et al.*, 2018a). A scanning laser Doppler vibrometer (LDV) [Polytec (Hörsching, Austria) UHF-120] was employed to characterize the displacement field of the SAWs generated by these broadband IDTs. This heterodyne device measures the out-of-plane vibrational component in the frequency range from direct current (DC) to 1.2 GHz (Smagin *et al.*, 2017).

To demonstrate the very high sensitivity of SAWs to the presence of extremely thin layers or films, two layer-on-substrate structures comprising 20 and 50 nm thick chromium thin films on a 1 mm thick silicon (111) substrate were studied. Given the SAW propagation velocities (of the first Rayleigh wave mode) between 4543 m/s (in the $[1\bar{1}0]$ direction) and 4738 m/s (in the $[11\bar{2}]$ direction), the wavelengths were between 17 and 50 μm in the $[1\bar{1}0]$ direction and between 18 and 52 μm in the $[11\bar{2}]$ direction for the frequency range between 90 and 260 MHz. Thus, the 20 nm layer was 900–2600 times smaller than the SAW wavelengths, and the 50 nm layer was 360–1040 times smaller than the SAW wavelengths. However, it is shown (Figs. 2 and 3) that these waves are indeed sensitive to coatings with thicknesses over 1000 times smaller than the wavelength.

For the measurements, 577 and 927 detection points were recorded at coordinate increments of 57.2 and 35.6 μm between each detection point for the samples coated with 50 and 20 nm of chromium, respectively. As the frequency range was between 90 and 260 MHz, the attenuation was not too strong (unlike the attenuation of waves propagating at frequencies around GHz or several GHz). It was then possible to propagate waves over several tens of millimeters and record the associated displacements over a sufficient length to obtain accurate results on experimental dispersion curves (total measured propagation path $L \approx 33$ mm). These experimental dispersion curves were obtained from the displacements recorded at the detection points and the slant stack transform (Ambrozinski *et al.*, 2014). There are several methods available to obtain the phase velocity dispersion, and when considering exploiting the dispersion phenomena of the first Rayleigh mode, it is possible, for example, to apply a wavelet transform to signals corresponding to different propagation distances (Everett, 2013; Rose, 2004; Viktorov, 1967). Phase velocities can also be obtained using a

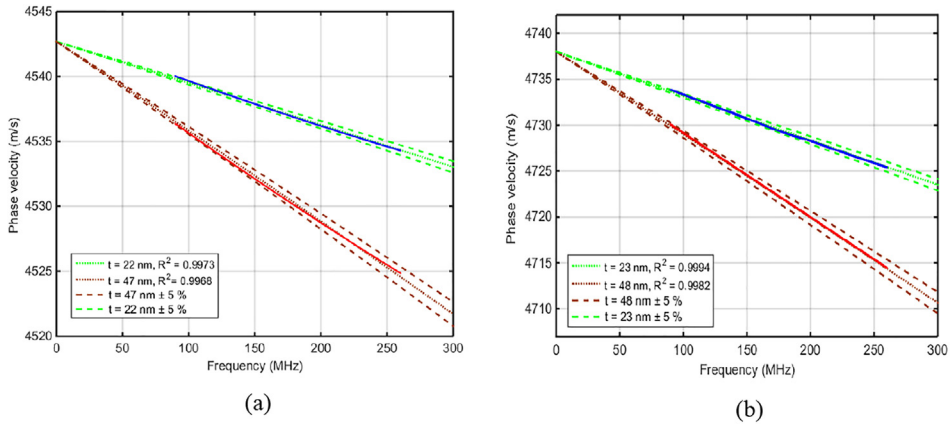

Fig. 2. Dispersion curves for 20 and 50 nm chromium layers on silicon in the $[1\bar{1}0]$ direction (a) and in the $[11\bar{2}]$ direction (b). Shown are experimental curves (solid lines), theoretical curves (dotted lines), and theoretical dispersion curves ± 5% of the estimated thickness (dashed lines).

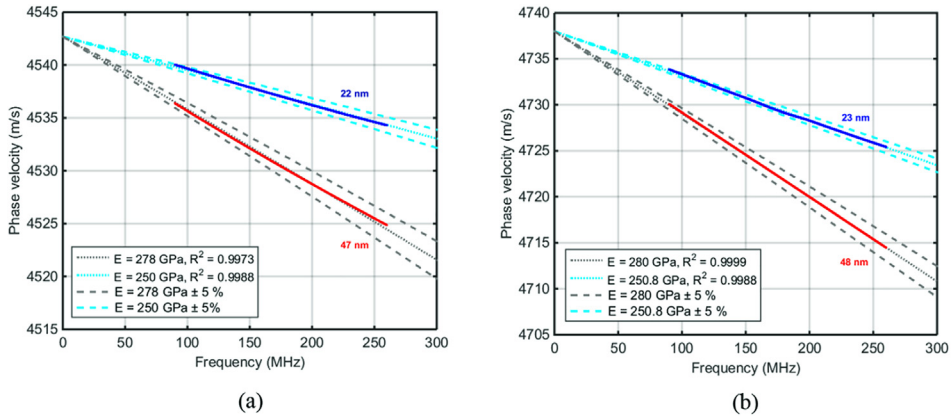

Fig. 3. Theoretical and experimental dispersion curves for 20 and 50 nm chromium layers on silicon and inversion results for Young's modulus in the $[1\bar{1}0]$ direction (a) and in the $[11\bar{2}]$ direction (b).

two-dimensional fast Fourier transform applied to time signals recorded at uniformly spaced distances (Lefevre *et al.*, 2010; Nayfeh, 1991). In this work, it was decided to use a fast and efficient alternative method to estimate velocities with high accuracy. Well known to geophysicists, the slant stack transform is used to determine the velocity of waves propagating in a dispersive medium (Askari *et al.*, 2012; Piwakowski *et al.*, 2004.; Yilmaz, 2001). In terms of precision, the results obtained using this method are as good as those of the other methods [two-dimensional fast Fourier transform (2DFFT), wavelet] (Ambrozinski *et al.*, 2014) while also providing the possibility of observing the dispersion curves directly. The slant stack method allows the precise determination of the phase velocity dispersion curves from displacements measured at different spatially distributed points. It is known as the p-ω transformation or oblique summation. Signal processing using this transform allows the phase velocity to be determined as a function of frequency. The method is detailed in particular for the case of Rayleigh waves (Abraham *et al.*, 2012; Askari *et al.*, 2012). The procedure for measuring the velocity V_R of Rayleigh waves as a function of frequency consists in calculating the maximum of the function $A(V)$ at the output of a correlator that measures and compensates for the delays between the signals detected by the vibrometer at positions 1, 2, N. In other words, a velocity band is defined such that $V_{\min} < V_R < V_{\max}$ and then $A(V)$ is determined. $A(V)$ is a function of the velocity V; therefore, the velocity for which the function is maximum corresponds to the measured wave velocity for the frequency f_0 under consideration. The function $A(V)$ is defined by (Piwakowski *et al.*, 2004),

$$A(V)_{\langle V, f_0 \rangle} = S(f_0)N\left|\frac{\sin\left(N\Delta x\pi f_0\left(\frac{1}{V}-\frac{1}{V_R}\right)\right)}{\left[N\cdot\sin\left(\Delta x\pi f_0\left(\frac{1}{V}-\frac{1}{V_R}\right)\right)\right]}\right|, \quad (1)$$

where Δx is the distance between the measurement points, f_0 is the frequency, V_R is the measured wave velocity, N is the number of measurement points, V is the wave velocity (considered as variable), and S is the constant resulting from the cross correlation of all the signals received.

Figure 2 presents the experimental dispersion curves (solid line) of wave propagation in the 20 and 50 nm thick chromium layers in the $[1\bar{1}0]$ direction [Fig. 2(a)] and in the $[11\bar{2}]$ direction [Fig. 2(b)]. The variations in velocity observed were on the order of 5–30 m/s depending on the case. The thickness of the chromium layers could, thus, be determined by inversion from these experimental dispersion curves (obtained between 90 and 260 MHz). This was achieved for thicknesses between 10 and 30 nm and between 40 and 60 nm with an increment of 1 nm. The inversion results for the two propagation directions indicated 22 and 23 nm for the thinnest layer and 47 and 48 nm for the second thin layer.

From these data, the theoretical dispersion curves were plotted (dotted lines) between 0 and 300 MHz (Fig. 2). The theoretical and experimental dispersion curves are almost identical (the R^2 regression coefficient is very close to 1 in the 90–260 MHz frequency band). The observed dispersion phenomenon is more pronounced for higher frequencies. Finally, to highlight the interest of the high frequency generation, the theoretical dispersion curves $\pm$ 5% of the estimated thickness (addition of 5% to or subtraction of 5% from the estimated thickness) have been plotted (dotted lines). This shows that for a thickness of 50 nm and frequencies below 150 MHz, it is quite difficult to distinguish a thickness variation within 5%. For a thickness of 20 nm, it is necessary to exceed 200 MHz to be able to make this distinction.

The results obtained in terms of thickness after inversion for the samples are very similar in both the $[1\bar{1}0]$ and $[11\bar{2}]$ directions of SAW propagation on the surface of the (111) silicon wafers. This indicates the good reproducibility and robustness of this ultrasonic method, as well as its good sensitivity to the dimensional properties (thickness) of the layers. In addition to the layer thickness, the method also shows that it is sensitive to the mechanical properties of the

silicon substrate (111), taking into account its anisotropic structure. The Young's modulus and Poisson's ratio of the substrate were 142.7 and 155.7 GPa and 0.26 and 0.27 in the propagation directions $[1\bar{1}0]$ and $[11\bar{2}]$, respectively. The inversion results of 22 and 23 nm for the thinner layer and 47 and 48 nm for the second thin layer for the two propagation directions also demonstrate that although a significant part of the energy is localized in the substrate, the thickness estimates are not affected by the elastic characteristics of the substrate.

Figure 3 presents the experimental dispersion curves (solid line) of wave propagation in the 20 and 50 nm thick chromium layers in the $[1\bar{1}0]$ direction [Fig. 3(a)] and in the $[11\bar{2}]$ direction [Fig. 3(b)]. Young's moduli of the chromium layers can be determined by inversion from the variations in velocity observed. Young's moduli were, therefore, determined by inversion from these experimental dispersion curves (obtained between 90 and 260 MHz). This was achieved for Young's moduli between 200 and 350 GPa with an increment of 1 GPa. The inversion results for the two respective propagation directions were 250 and 251 GPa for the 22 nm layer and 278 and 280 GPa for the 47 nm layer.

From these data, the theoretical dispersion curves were plotted (dotted lines) between 0 and 300 MHz. The theoretical and experimental dispersion curves are almost identical. Finally, to highlight the interest of the high frequency, the theoretical dispersion curves $\pm$ 5% of the estimated thickness were plotted (dashed lines). This shows that for a thickness of 50 nm and frequencies below 150 MHz, it is quite difficult to distinguish a thickness within 5%. For a thickness of 20 nm, it is necessary to exceed 200 MHz to be able to make this distinction.

Concerning the results in terms of Young's modulus and Poisson's ratio of the ultrathin chromium layers, the values obtained on the same sample in both directions $[1\bar{1}0]$ and $[11\bar{2}]$ show a very small difference in Young's modulus and an almost identical Poisson's ratio values. For the sample with a 50 nm Cr layer, the estimated Young's modulus and Poisson's ratio were (278 GPa, 0.16) and (280 GPa, 0.16) in the $[1\bar{1}0]$ and $[11\bar{2}]$ directions, respectively. For the sample with a 20 nm Cr layer, the estimated Young's modulus and Poisson's ratio were (250 GPa, 0.19) and (250.8 GPa, 0.19) in the $[1\bar{1}0]$ and $[11\bar{2}]$ directions, respectively. These results show the sensitivity of the method to the elastic properties of the layers. The difference in Young's modulus (E) observed (about 10%) between the two ultrathin chromium layers (278 GPa for the 50 nm layer and 250 GPa for the 20 nm layer) can be explained by the scaling effect on the properties of the submicrometer chromium thin films.

To explain this difference in the estimation of Young's modulus, the microstructure of the chromium thin films was studied using atomic force microscopy (AFM). AFM images of the surface morphology and surface roughness of the samples (H, 20 nm Cr; G, 50 nm Cr) are shown in Fig. 4. In these figures, the branching areas correspond to silicon particles from the cleavage. The two AFM images presented in Fig. 4 reveal that the surface roughness (R_a) is equal to 0.7 nm for the 20 nm Cr layer and 2.1 nm for the 50 nm Cr layer. The surface roughness of $R_a = 0.7$ [20 nm Cr/Si(111)] tells us that the surface is smooth and uniform and, therefore, that the granulometric structures change little and their distribution is quite homogeneous. For the sample with a roughness of $R_a = 2.1$ nm [50 nm Cr/Si (111)], the grain size is probably larger than that of the other sample [20 nm Cr/Si (111)]. This is probably due to the formation of larger surface crystals. Indeed, the grain size in thin films becomes larger as the thickness of the thin film increases, and crystallization increases as the thickness of the thin film increases. Schiøtz and Jacobsen (2003) studied this phenomenon for a series of measurements on several materials. They observed that the increase in yield strength is inversely proportional to the square root of the grain size; the other quantities followed a similar relationship. This relationship, known as the Hall–Petch relationship, is well established experimentally from millimeter-size grains to the submicron scale (Schiøtz and Jacobsen, 2003).

In conclusion, this research importantly highlighted the sensitivity of SAWs to very thin layers and showed that, by exciting these waves over a large frequency range, it is possible to verify this sensitivity by observing the dispersion phenomenon. Ultimately, by exploiting the variation in propagation velocities, it was possible to characterize the layers. The dispersion phenomenon could be highlighted despite the substantial ratio between the wavelength and the layer thickness. It was also highlighted that the device was able to excite the SAWs correctly over a large frequency band and detect the displacements generated by these waves. Finally, it was possible to determine the characteristics of the layers (thickness, Young's modulus) from the dispersion curve plots. Thus, a future prospect of this work concerns layers-on-substrate structure characterization (Mittal, 1976; O'Connor *et al.*, 1992; Oliver and Pharr, 1992; Ollendorf and Schneider, 1999).

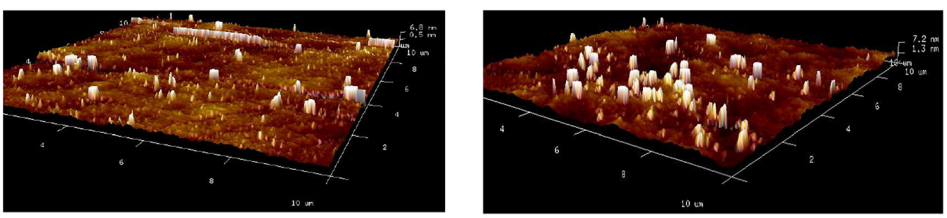

(a) (b)

Fig. 4. Three-dimensional (3D) AFM images of chromium thin films deposited on a silicon substrate (111) 20 nm Cr (a) and 50 nm Cr (b).

Acknowledgments

This work was accomplished within the framework of the ELSAT2020 project co-financed by the European Union through the European Regional Development Fund, the French government, and the Hauts-de-France Regional Council. This work was also supported by the French RENATECH network.

References and links

Abraham, O., Piwakowski, B., Villain, G., and Durand, O. (**2012**). "Non-contact, automated surface wave measurements for the mechanical characterisation of concrete," Construct. Build. Mater. **37**, 904–915.

Ambrozinski, L., Piwakowski, B., Stepinski, T., and Uhl, T. (**2014**). "Evaluation of dispersion characteristics of multimodal guided waves using slant stack transform," NDT&E Int. **68**, 88–97.

Askari, R., Ferguson, R. J., and DeMeersman, K. (**2012**). "Estimation of group velocity using slant stack generalized transform-based method," in *Proceedings of GeoConvention 2012: Vision*, May 14–18, Toronto, Canada.

Deboucq, J., Duquennoy, M., Ouaftouh, M., Jenot, F., Carlier, J., and Ourak, M. (**2011**). "Development of interdigital transducer sensors for non-destructive characterization of thin films using high frequency Rayleigh waves," Rev. Sci. Instrum. **82**, 064905.

Duquennoy, M., Ouaftouh, M., Deboucq, J., Lefebvre, J.-E., Jenot, F., and Ourak, M. (**2012**). "Influence of a superficial field of residual stress on the propagation of surface waves—Applied to the estimation of the depth of the superficial stressed zone," Appl. Phys. Lett. **101**, 234104.

Everett, M. E. (**2013**). *Near-Surface Applied Geophysics*, 1st ed. (Cambridge University, Cambridge, UK).

Fall, D., Compoint, F., Duquennoy, M., Piombini, H., Ouaftouh, M., Jenot, F., Piwakowski, B., Belleville, P., and Ambard, C. (**2016**). "Surface acoustic wave characterization of optical sol-gel thin layers," Ultrasonics **68**, 102–107.

Fall, D., Duquennoy, M., Ouaftouh, M., Smagin, N., Piwakowski, B., and Jenot, F. (**2017**). "Generation of broadband surface acoustic waves using a dual temporal-spatial chirp method," J. Acoust. Soc. Am. **142**, EL108–EL112.

Fall, D., Duquennoy, M., Ouaftouh, M., Smagin, N., Piwakowski, B., and Jenot, F. (**2018a**). "Optimization of interdigital transducers for the generation of surface acoustic waves over a large bandwidth (20–125 MHz)," Sens. Actuators A Phys. **273**, 303–310.

Fall, D., Duquennoy, M., Ouaftouh, M., Smagin, N., Piwakowski, B., and Jenot, F. (**2018b**). "Non-destructive characterization of surfaces and thin coatings using a large-bandwidth interdigital transducer," Rev. Sci. Instrum. **89**, 124901.

Goossens, J., Leclaire, P., Xu, X., Glorieux, C., Martinez, L., Sola, A., Siligardi, C., and Cannillo, V. (**2007**). "Surface acoustic wave depth profiling of a functionally graded material," J. Appl. Phys. **102**, 053508.

Hess, P. (**2009**). "Determination of linear and nonlinear mechanical properties of diamond by laser-based surface acoustic waves," Diamond Relat. Mater. **18**, 186–190.

Lakestani, F., Coste, J.-F., and Denis, R. (**1995**). "Application of ultrasonic Rayleigh waves to thickness measurement of metallic coatings," NDT&E Int. **28**, 171–178.

Lefevre, F., Jenot, F., Ouaftouh, M., Duquennoy, M., and Ourak, M. (**2010**). "Laser generated guided waves and finite element modeling for the thickness gauging of thin layers," Rev. Sci. Instrum. **81**, 034901.

Lomonosov, A., Mayer, A. P., and Hess, P. (**2001**). "Laser controlled surface acoustic waves," in *Handbook of Elastic Properties of Solids, Liquids, and Gases* (Academic, New York), Vol. 1, pp. 137–185.

Mittal, K. (**1976**). *Adhesion Measurement of Thin Films, Thick Films, and Bulk Coatings* (American Society for Testing and Materials, Philadelphia).

Nayfeh, A. H. (**1991**). "The general problem of elastic wave propagation in multilayered anisotropic media," J. Acoust. Soc. Am. **89**, 1521–1531.

O'Connor, D. J., Sexton, B. A., and Smart, R. S. C. (**1992**). *Surface Analysis Methods in Materials Science* (Springer-Verlag, Berlin).

Oliver, W. C., and Pharr, G. M. (**1992**). "An improved technique for determining hardness and elastic modulus using load and displacement sensing indentation experiments," J. Mater. Res. **7**, 1564–1583.

Ollendorf, H., and Schneider, D. (**1999**). "A comparative study of adhesion test methods for hard coatings," Surf. Coat. Technol. **113**, 86–102.

Piwakowski, B., Goueygou, M., Fnine, A., and Buyle, B. (**2004**). "P-τ transformation as the efficient tool for determination of the velocity dispersion characteristics in complex structures," in *Proceedings of the 16th World Conference on NDT (WCNDT 2004)*, August 30–September 3, Montreal, Canada.

Rose, J. L. (**2004**). *Ultrasonic Waves in Solid Media* (Cambridge University, Cambridge, UK).

Ruiz, A., and Nagy, P. B. (**2003**). "SAW dispersion measurements for ultrasonic characterization of surface treated metals," Instrum. Mes. Metrol. **3**, 59.

Schiøtz, J., and Jacobsen, K. W. (**2003**). "A maximum in the strength of nanocrystalline copper," Science **301**, 1357–1359.

Schneider, D., Hammer, R., and Jurisch, M. (**1999**). "Non-destructive testing of damage layers in GaAs wafers by surface acoustic waves," Semicond. Sci. Technol. **14**, 93–98.

Smagin, N., Djoumi, L., Herth, E., Vanotti, M., Fall, D., Blondeau-Patissier, V., Duquennoy, M., and Ouaftouh, M. (**2017**). "Fast time-domain laser Doppler vibrometry characterization of surface acoustic waves devices," Sens. Actuators A Phys. **264**, 96–106.

Tancrell, R. H., and Holland, M. G. (**1971**). "Acoustic surface wave filters," Proc. IEEE **59**, 393–409.

Tittmann, B. R., Ahlberg, L. A., Richardson, J. M., and Thompson, R. B. (**1987**). "Determination of physical property gradients from measured surface wave dispersion," IEEE Trans. Ultrason. Ferroelectr. Freq. Control **34**, 500–507.

Toda, K., Sugizaki, G., Takenaka, T., and Sakata, K. (**1994**). "A technique for measuring strain in layered structure media," Sens. Actuators A Phys. **43**, 213–216.

Viktorov, I. A. (**1967**). *Rayleigh and Lamb Waves* (Springer, New York).

Warren, P. D., Pecorari, C., Kolosov, O. V., Roberts, S. G., and Briggs, G. A. D. (**1996**). "Characterization of surface damage via surface acoustic waves," Nanotechnology **7**, 295.

Wu, T.-T., Chen, Y.-Y., Huang, G.-T., and Chang, P.-Z. (**2005**). "Evaluation of elastic properties of submicrometer thin films using slanted finger interdigital transducers," J. Appl. Phys. **97**, 073510.

Yilmaz, Ö. (**2001**). *Seismic Data Analysis: Processing, Inversion, and Interpretation of Seismic Data* (Society of Exploration Geophysicists, Houston, TX).